
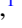

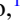



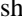
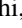

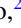
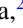






## Light-induced magnetization driven by interorbital charge motion in the spin-orbit assisted Mott insulator $\alpha$ -RuCl<sub>3</sub>

T. Amano <sup>1</sup>, Y. Kawakami <sup>1</sup>, H. Itoh <sup>1</sup>, K. Konno <sup>1</sup>, Y. Hasegawa <sup>1</sup>, T. Aoyama <sup>1</sup>, Y. Imai <sup>1</sup>, K. Ohgushi <sup>1</sup>, Y. Takeuchi <sup>1</sup>, Y. Wakabayashi <sup>1</sup>, K. Goto <sup>2</sup>, Y. Nakamura <sup>2</sup>, H. Kishida <sup>2</sup>, K. Yonemitsu <sup>3</sup> and S. Iwai <sup>1,\*</sup>

<sup>1</sup>Department of Physics, Tohoku University, Sendai 980-8578, Japan

<sup>2</sup>Department of Applied Physics, Nagoya University, Nagoya 464-8603, Japan

<sup>3</sup>Department of Physics, Chuo University, Tokyo 112-8551, Japan

 (Received 1 November 2021; revised 10 June 2022; accepted 8 July 2022; published 19 August 2022)

In a honeycomb-lattice spin-orbit assisted Mott insulator  $\alpha$ -RuCl<sub>3</sub>, ultrafast magnetization is induced by circularly polarized excitation below the Mott gap. Photocarriers play an important role, which are generated by turning down the synergy of the onsite Coulomb interaction and the spin-orbit interaction realizing the insulator state. An ultrafast 6 fs measurement of photocarrier dynamics and a quantum mechanical analysis clarify the mechanism, according to which the magnetization emerges from a coherent charge motion between different  $t_{2g}$  orbitals ( $d_{yz}$ - $d_{xz}$ - $d_{xy}$ ) of Ru<sup>3+</sup> ions. This ultrafast magnetization is weakened in the antiferromagnetic (AFM) phase, which is opposite to the general tendency that the inverse Faraday effect is larger in AFM compounds than in paramagnetic ones. This temperature dependence indicates that the interorbital charge motion is affected by pseudospin rotational symmetry breaking in the AFM phase.

DOI: [10.1103/PhysRevResearch.4.L032032](https://doi.org/10.1103/PhysRevResearch.4.L032032)

Emergent properties of strongly correlated charges and spins enable us to expect a pathway for light-induced spatial/time-reversal symmetry breaking [1–6]. Spin-orbit assisted Mott insulators exhibiting quantum frustrations [7–10] are promising candidates for realizing light-induced magnetization (or equivalently time-reversal symmetry breaking) because of their charge-orbital-spin entanglement. Note that the materials for light-induced magnetization have been discussed mainly in antiferromagnets (AFMs) or weak ferromagnets [11–14].

The layered insulator  $\alpha$ -RuCl<sub>3</sub> with a honeycomb lattice [left side of Fig. 1(a)] has attracted much attention as a spin-orbit assisted Mott insulator [8–10,15–19]. The strong spin-orbit interaction (SOI) splits the  $t_{2g}$  states of a Ru<sup>3+</sup> ion into pseudospins  $J_{\text{eff}} = \frac{1}{2}$  and  $\frac{3}{2}$ . Thus, the Mott insulating state of this compound is realized by the synergy of the onsite Coulomb interaction  $U$  and the SOI [20]. In the edge-sharing octahedron [right side of Fig. 1(a)], no long-range order is allowed if only the bond-dependent anisotropic exchange interaction (Kitaev interaction) exists between the  $J_{\text{eff}} = \frac{1}{2}$  pseudospins on the honeycomb lattice. In fact, magnetic orders are not detected down to  $T_N$ , although a zigzag AFM order in the honeycomb plane ( $ab$  plane) is reported below  $T_N = 7$ –14 K which depends on the volume fractions of  $R\bar{3}$  and  $C2/m$  (Supplemental Material 1 [21]) [22–30]. Here, intersite

hopping  $t$  between different  $t_{2g}$  orbitals (such as  $d_{xz}$ - $d_{yz}$ ) of Ru ions is essential. Because of this characteristic intersite hopping, peculiar charge and spin dynamics on the ultrafast time scale are expected. Another important characteristic is in-gap states below the Mott-Hubbard transition ( $E_{\text{gap}} = 1.2$  eV < 50 K [31–35]) [Fig. 1(b)] that were discussed in terms of orbital excitations influenced by the SOI. They were recently assigned to excitations from  $J_{\text{eff}} = \frac{3}{2}$  to  $\frac{1}{2}$  states [lower inset of Fig. 1(b)] [32–34]. The in-gap states have a broad and overlapped  $\varepsilon_2$  spectrum in the range 0.2–0.9 eV [Fig. 1(b)]. The three peaks (0.31, 0.53, and 0.72 eV) roughly reflect different numbers of  $J_{\text{eff}} = \frac{3}{2}$  holes substituting for  $J_{\text{eff}} = \frac{1}{2}$  holes in the Mott insulating background with one  $J_{\text{eff}} = \frac{1}{2}$  hole at each site [32]. Because of the spin-orbit assisted nature of this Mott insulator [20], an excitation of these spin-orbit coupled (SOC) in-gap states in  $\alpha$ -RuCl<sub>3</sub> may take advantage of charge degrees of freedom in light-induced phenomena.

In this letter, we report that a circularly polarized excitation below the Mott gap produces magnetization perpendicular to the honeycomb plane of  $\alpha$ -RuCl<sub>3</sub>. Ultrafast dynamics of photocarriers and a quantum many-body analysis show that the ultrafast magnetization is driven by the hopping  $t$  between different  $t_{2g}$  orbitals ( $d_{yz}$ - $d_{xz}$ ,  $d_{xz}$ - $d_{xy}$ , and  $d_{xy}$ - $d_{yz}$ ).

The samples used in this letter were prepared by the chemical vapor transport method [35]. We performed transient polarization rotation ( $\Delta\theta$ ) and transmission ( $\Delta T/T$ ) measurements for circularly polarized excitation using the pump-probe method with the time resolution of 100 fs. The probing spectral range covers 0.5–1.1 eV for the pump light with 0.30, 0.62, 0.89, and 1.55 eV. Here,  $\Delta R/R$  spectra are measured for excitations of 0.62 and 0.89 eV. In addition, we measure  $\Delta R/R$  with higher time-resolution by utilizing a carrier-envelope phase stabilized 6 fs

\*s-iwai@tohoku.ac.jp

Published by the American Physical Society under the terms of the [Creative Commons Attribution 4.0 International license](https://creativecommons.org/licenses/by/4.0/). Further distribution of this work must maintain attribution to the author(s) and the published article's title, journal citation, and DOI.

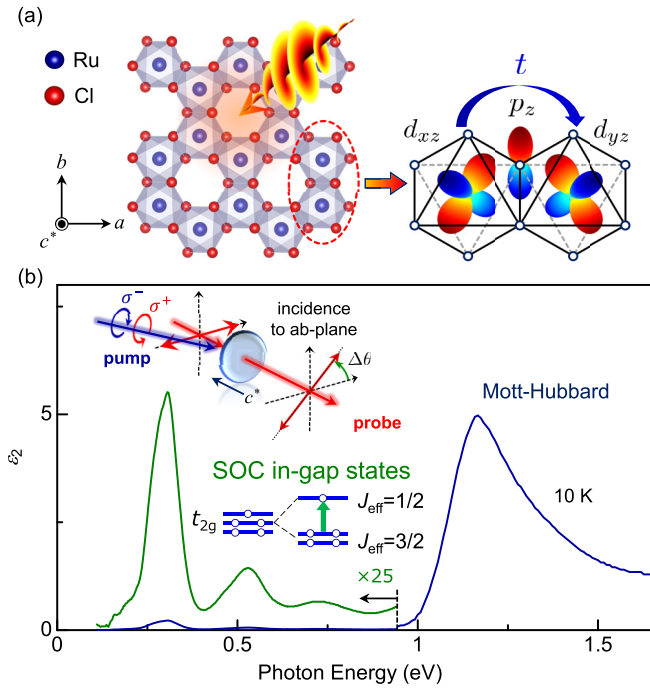


FIG. 1. (a) Honeycomb lattice of  $\alpha$ -RuCl<sub>3</sub> and hybridization between  $t_{2g}$  orbitals of Ru and ligand  $p_z$  orbital of Cl which causes hopping  $t$  between different  $t_{2g}$  orbitals (such as  $d_{xz}$ - $d_{yz}$ ). (b) Imaginary part of the permittivity spectrum in mid- and near-infrared regions [31]. The low-energy part  $< 0.9$  eV (magnified 25 times) is attributed to spin-orbit coupling (SOC) in-gap states [31–33]. The experimental configuration of the optomagneto measurement (polarization rotation induced by a circularly polarized pump pulse) and the excitation from  $J_{\text{eff}} = \frac{3}{2}$  to  $\frac{1}{2}$  states [32] are schematically shown.

near-infrared pulse for investigating ultrafast charge coherence [36,37].

The upper panel of Fig. 2(a) shows time evolutions of  $\Delta\theta$  (probe energy  $E_{\text{pr}} = 0.62$  eV,  $\parallel ab$  plane) induced by the circularly polarized pump pulse (pump energy  $E_{\text{pu}} = 0.89$  eV, intensity  $I_{\text{ex}} = 4$  mJ/cm<sup>2</sup>) at 4 K (dashed curves,  $T < T_N$ ) and 17 K (solid curves,  $T > T_N$ ). The helicity ( $\sigma^+$ ,  $\sigma^-$ ) of the pump pulse and the direction of the rotation angle are defined as those in the right-handed system [upper inset of Fig. 1(b)]. The helicity-dependent responses as large as  $4.5^\circ$ – $5.5^\circ$  within the time resolution ( $\sim 100$  fs) in Fig. 2(a) are attributed to the Faraday rotation reflecting an ultrafast magnetization perpendicular to the  $ab$  plane ( $\perp ab$ ) at both 4 and 17 K (Supplemental Material 2 [21]) [38]. The observation of such large  $\Delta\theta$  without any long-range order at 17 K contrasts with the ultrafast inverse-Faraday effect in AFM compounds [11–14]. The transient transmittance ( $\Delta T/T$ ) in the lower panel of Fig. 2(a) shows concomitant charge dynamics with a finite decay time, indicating real excitation of in-gap states. In fact,  $\Delta\theta$  normalized by the thickness ( $\sim 50$   $\mu\text{m}$ ) and  $I_{\text{ex}}$  (4 mJ/cm<sup>2</sup>) is 20 times larger than that of a prototypical AFM magnet NiO (111) ( $1.14^\circ$  for  $E_{\text{pu}} = 0.97$  eV,  $E_{\text{pr}} = 1.59$  eV,  $I_{\text{ex}} = 10$  mJ/cm<sup>2</sup>, thickness 100  $\mu\text{m}$  [14]). It is 400 times larger than that of a paramagnet terbium gallium garnet ( $0.15^\circ$  for  $E_{\text{pu}} = E_{\text{pr}} = 1.55$  eV,  $I_{\text{ex}} = 3.1$  mJ/cm<sup>2</sup>, thickness 1 mm [39]).

The temperature dependence of  $\Delta\theta$  at time delay ( $t_d$ ) of 0 ps in the upper panel of Fig. 2(b) shows an abrupt change near  $T_N = 7$  K. The reduction of  $\Delta\theta$  (of  $\sim 15\%$ ) below  $T_N$  indicates that the ultrafast magnetization ( $\perp ab$ ) is weakened in the AFM phase, which is opposite to the general tendency that the inverse Faraday effect is larger in AFM compounds than in paramagnetic ones. Above 20 K,  $\Delta\theta$  is insensitive to the temperature (Supplemental Material 3 [21]).

The helicity-independent slower component of  $\Delta\theta$  [ $\times 10$  for  $t_d > 1$  ps in Fig. 2(a)] is attributed to a melting of the AFM order (Supplemental Material 4 [21]) [40]. In fact,  $\Delta\theta$  at 10 ps drops near  $T_N$  [lower panel of Fig. 2(b)]. In contrast to the

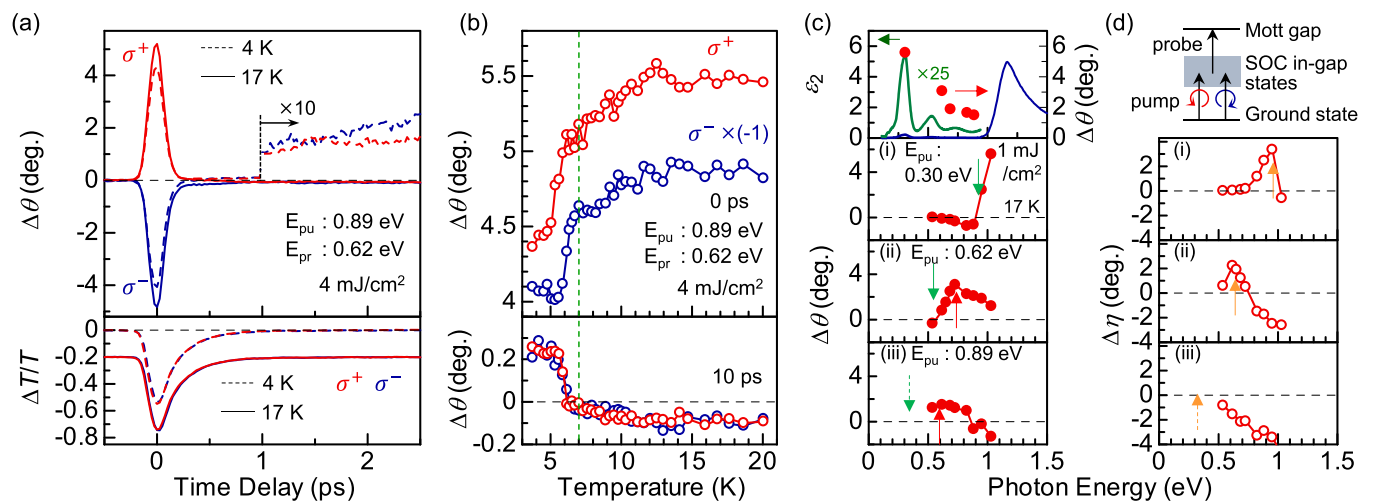


FIG. 2. (a) Time evolutions of  $\Delta\theta$  (upper panel) and transmittance ( $\Delta T/T$ ) (lower panel) of  $\alpha$ -RuCl<sub>3</sub> ( $E_{\text{pu}} = 0.89$  eV,  $I_{\text{ex}} = 4$  mJ/cm<sup>2</sup>,  $E_{\text{pr}} = 0.62$  eV,  $\parallel ab$  plane,  $\sigma^+$ : red curves,  $\sigma^-$ : blue curves) at 4 K (dashed curves) and 17 K (solid curves). (b) Temperature dependences of  $\Delta\theta$  at  $t_d = 0$  ps (upper panel) and at  $t_d = 10$  ps (lower panel). Optomagneto spectra (17 K) of (c)  $\Delta\theta$  and (d)  $\Delta\eta$  for (i)  $E_{\text{pu}} = 0.30$  eV, (ii)  $E_{\text{pu}} = 0.62$  eV, and (iii)  $E_{\text{pu}} = 0.89$  eV. The upper panel of (c) shows the imaginary permittivity spectrum [31] ( $\times 25$  for  $< 0.9$  eV). The maximum values of  $\Delta\theta$  for  $E_{\text{pu}} = 0.30$ – $0.89$  eV are shown by the red dots. A schematic illustration of the optomagneto two-step process is shown in the upper panel of (d).

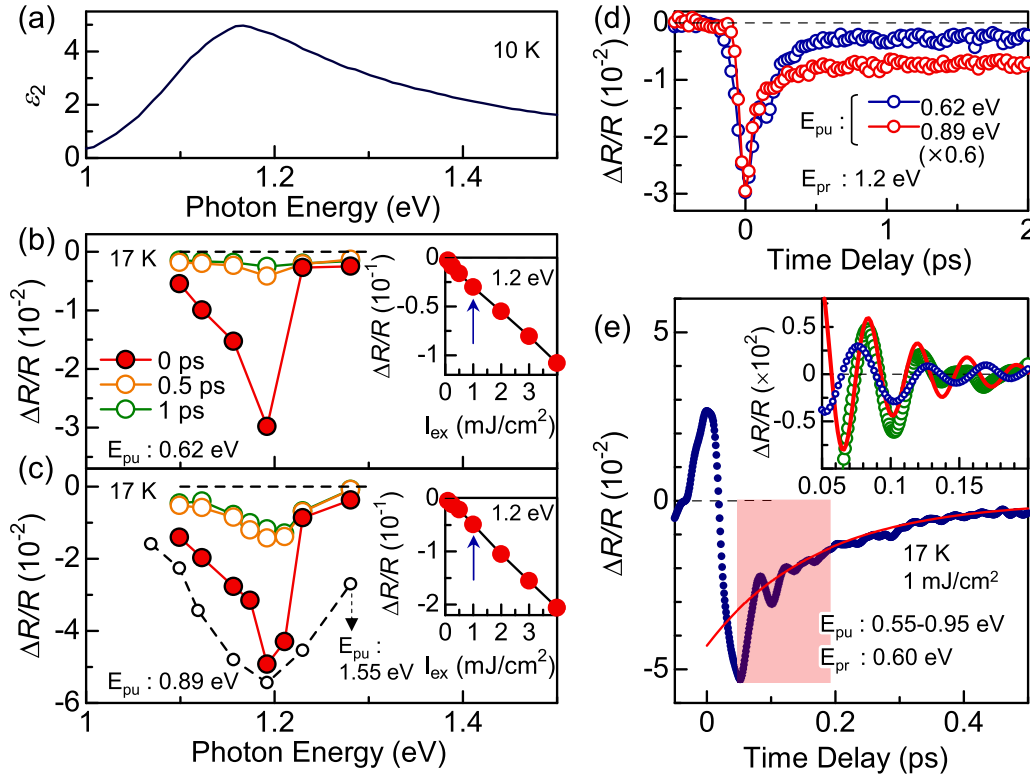


FIG. 3. (a) Imaginary part of the permittivity spectrum at 10 K [31] around the Mott gap.  $\Delta R/R$  spectra for (b)  $E_{pu} = 0.62$  eV and (c)  $E_{pu} = 0.89$  eV.  $I_{ex} = 1 \text{ mJ}/\text{cm}^2$ , 17 K,  $t_d = 0$  ps (red dots), 0.5 ps (orange circles), 1 ps (green circles). The insets of (b) and (c) show the  $I_{ex}$  dependence of  $\Delta R/R$  at  $E_{pr} = 1.2$  eV. The circles with the dashed curve in (c) show  $\Delta R/R$  for  $E_{pu} = 1.55$  eV ( $4 \text{ mJ}/\text{cm}^2$ ,  $\times 0.17$ , 4 K,  $t_d = 0$  ps). (d) Time profiles of  $\Delta R/R$  ( $E_{pr} = 1.2$  eV) for  $E_{pu} = 0.62$  eV (blue circles) and  $E_{pu} = 0.89$  eV (red circles  $\times 0.6$ ). (e) Time profile of  $\Delta R/R$  measured by using a 6 fs near-infrared pulse ( $E_{pu} = 0.55-0.95$  eV,  $E_{pr} = 0.60$  eV (with polarization perpendicular to that of the pump pulse),  $I_{ex} = 1.0 \text{ mJ}/\text{cm}^2$ , 17 K). The red curve shows exponential decay with a time constant of 0.17 ps. The oscillating component is shown in the inset [green circles: 17 K, blue circles 300 K, red curve: oscillation with a period of 36 fs (Supplementary 9 [21])].

temperature-sensitive nature of  $\Delta\theta$ ,  $\Delta T/T$  do not indicate any temperature dependence near  $T_N$  [as shown in the lower panel of Fig. 2(a)], showing that the temperature dependence of  $\Delta\theta$  is not attributed to a change in the steady-state absorption coefficient ( $\alpha$ ) at  $E_{pu}$ . A large  $\Delta T/T \sim 0.6$  ( $\Delta\alpha/\alpha$  of 0.3) reflects excited carrier dynamics which will be discussed later along with  $\Delta R/R$  around the Mott-Hubbard band.

To investigate a mechanism of light-induced magnetization under the excitation below the Mott gap, we measure optomagneto spectra [ $\Delta\theta(E_{pr})$ : rotation angle and  $\Delta\eta(E_{pr})$ : ellipticity] by changing  $E_{pu}$ . Figures 2(c) and 2(d) show the  $\Delta\theta(E_{pr})$  and  $\Delta\eta(E_{pr})$  spectra, respectively, for (i)  $E_{pu} = 0.30$  eV, (ii)  $E_{pu} = 0.62$  eV, and (iii)  $E_{pu} = 0.89$  eV ( $I_{ex} = 1 \text{ mJ}/\text{cm}^2$ ). As shown in (i) and (ii) of Figs. 2(c) and 2(d), the energy where  $\Delta\theta = 0$  ( $\Delta\theta = 0$  intersection: green arrow) is equal to the energy where  $\Delta\eta$  has a peak ( $\Delta\eta$  peak: orange arrow), and it is  $\sim 0.9$  eV for  $E_{pu} = 0.30$  eV and  $\sim 0.6$  eV for  $E_{pu} = 0.62$  eV. The  $\Delta\theta = 0$  intersection and the  $\Delta\eta$  peak correspond to the resonance energy  $E_{res}$  in the magneto-optical spectrum  $\theta = \frac{\omega l}{2cn} \text{Im}(\epsilon_{xy})$  and  $\eta = -\frac{\omega l}{2cn} \text{Re}(\epsilon_{xy})$  ( $\epsilon_{xy}$ : off-diagonal component of the permittivity,  $n$ : refractive index, and  $l$ : sample thickness) for the single resonance oscillator [41]. The red dots in the upper panel of Fig. 2(c) show the maximum values in the respective  $\Delta\theta$  spectra (i.e., the excitation spectrum of  $\Delta\theta$ ) for  $E_{pu} =$

0.30–0.89 eV. Since a probe light with energy  $>0.9$  eV is not transmitted, a true maximum cannot be detected for a pump light  $\leq 0.3$  eV. Thus, the excitation spectrum of  $\Delta\theta$  is underestimated at  $E_{pu} = 0.3$  eV. Even in this limited situation, the tendency of the excitation spectrum in the upper panel of Fig. 2(c) is like that of  $\epsilon_2$  in the sense that  $\Delta\theta$  becomes large for lower excitation energies. The ultrafast magnetization is absent for the excitation above the Mott gap (Supplemental Material 5 [21]). It is noteworthy that  $E_{pu} + E_{res} \cong E_{gap} = 1.2$  eV is satisfied for  $E_{pu} = 0.30$  and 0.62 eV. This relation suggests that a third-order nonlinear [ $\chi^{(3)}$ ] process ( $E_{pu} + E_{pr} = E_{gap}$ ) through a virtual excitation by pump light may partially contribute, although photocarriers are generated.

These results show that the probe pulse further excites the in-gap states during their lifetime ( $<100$  fs) to a state just above the Mott gap. This lifetime is comparable with the inverse of the bandwidth ( $\sim 100$  meV) of each peak in the  $\epsilon_2$  spectrum [Fig. 1(b)] and is supported by the results of the ultrafast measurement using a 6 fs pulse [Fig. 3(e)]. The large  $\Delta\theta$  in  $\alpha\text{-RuCl}_3$  is characteristic of the real excitation below the Mott gap and the two-step excitation at  $E_{pu} + E_{pr}$  which is resonant to the Mott gap.

The insulating state is affected by the excitation below the Mott gap, as shown in the transient reflectivity ( $\Delta R/R$ ) spectra for  $E_{pu} = 0.62$  eV [Fig. 3(b)] and 0.89 eV [Fig. 3(c)]. The

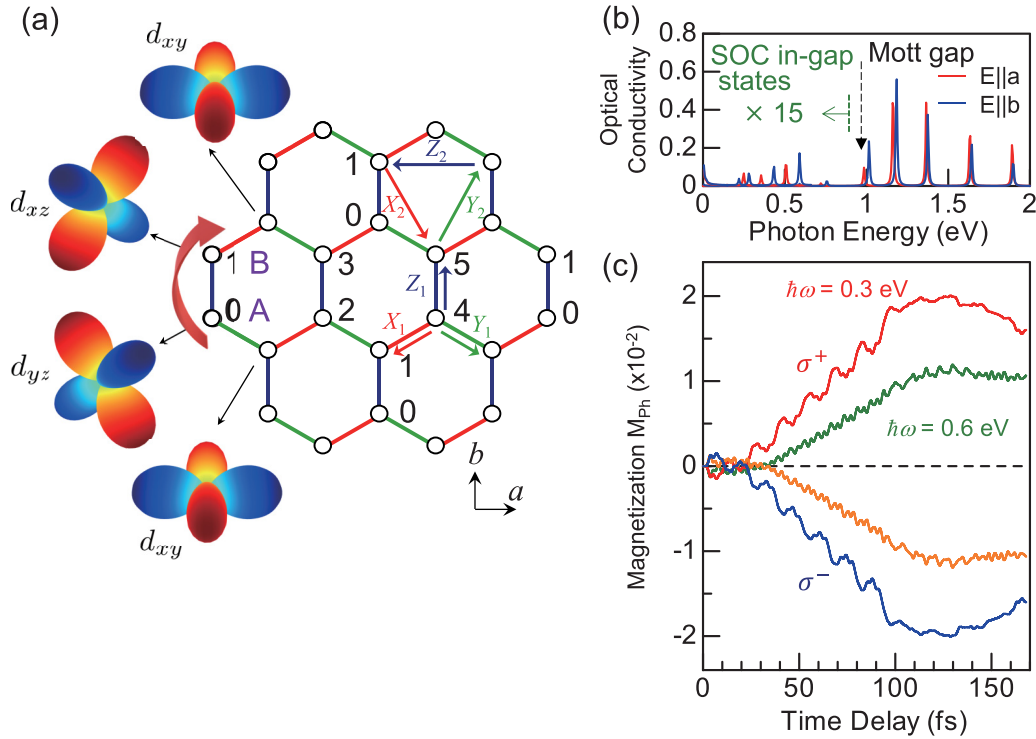


FIG. 4. (a) Honeycomb lattice structure of  $\alpha$ -RuCl<sub>3</sub> used in the calculation. It has 3 u.c., each of which consists of two sites A and B. Periodic boundary conditions are used to maintain the threefold symmetry.  $X_1, Y_1$ , and  $Z_1$  connect nearest-neighbor sites, and  $X_2, Y_2$ , and  $Z_2$  connect next-nearest-neighbor sites. (b) Calculated optical conductivity spectra for the ground state (red and blue curves are used for  $||a$ ,  $||b$ ). The spectra  $< 0.9$  eV are magnified by 15 times. (c) Calculated time profiles of photoinduced magnetization in the direction of  $\perp ab$ . An electric field amplitude times intersite distance  $F$  (V) of 0.2 (an electric field amplitude of 5.8 MV/cm), frequencies  $\hbar\omega$  (eV) of 0.3, 0.6, and a pulse width of 96 fs are used.

steady-state reflectivity ( $R$ ) is shown in Fig. 3(a) for reference. The bleaching near the Mott-Hubbard transition at 1.2 eV is clearly detected, where the two-photon ( $2 \times E_{\text{pu}}$ ) absorption of the pump pulse is ruled out as the origin of the bleaching because of the linear dependence of  $\Delta R/R$  on  $I_{\text{ex}}$  [insets of Figs. 3(b) and 3(c)]. This fact shows that photocarriers are generated by the excitation below the Mott gap as well as the excitation above the Mott gap [black circles with dashed curve in Fig. 3(c)] [40,42] (Supplemental Material 6 [21]). This is consistent with the fact that the Mott insulating state of this compound is realized by the synergy of the onsite Coulomb interaction  $U$  and the SOI [20] (Supplemental Material 7 [21]). Analyses of the time profiles of  $\Delta R/R$  [Fig. 3(d)] by using a multi-exponential function (Supplemental Material 8 [21]) show that the components with the decay time constants of  $< 0.1$  ps (50–60%) and 0.25 ps ( $\sim 35\%$ ) are dominant. They are consistent with the time constants of  $\Delta T/T$  [Fig. 2(a)], confirming that the time profiles of  $\Delta T/T$  reflect the photocarrier dynamics (Supplemental Material 8 [21]).

The fast ( $< 0.1$  ps) component of the recovery of  $\Delta R/R$  is comparable with that of  $\Delta\theta$  in Figs. 2(a) and 2(b). This fact indicates that the ultrafast magnetization is induced by the photocarriers. The early-stage dynamics of the photocarriers are captured by the  $\Delta R/R$  measurement utilizing a 6 fs pulse ( $E_{\text{pu}} = 0.55\text{--}0.95$  eV,  $E_{\text{pr}} = 0.60$  eV) [36], although a coherent polarization effect observed at  $t_d = -0.05$  to 0.05 ps is nonessential to the photocarrier dynamics. In addition to the exponential function with a time constant of 0.17 ps (red line)

which is roughly equal to those in Fig. 3(d) (0.25 ps), the time profile of  $\Delta R/R$  in Fig. 3(e) has an oscillating component with a period of 36 fs, as shown by the green circles in the inset (Supplemental Material 9 [21]). Since the oscillating period [ $36$  fs =  $h/(0.11$  eV)] corresponds to the energies of the intersite hopping (0.1–0.2 eV) [43–45], the oscillation would be related to the intersite hopping processes including the interorbital one. Note that phonon energies are restricted to a range  $< 40$  meV [15–17,34]. Such coherent charge motions are often realized by the simultaneous application of a light-field force to many electrons that are correlated by the Coulomb interaction [46,47] (Supplemental Material 9 [21]). The dephasing time of the oscillation (60 fs; Supplemental Material 9 [21]) reflecting the coherence time of the intersite charge motion is approximately equal to the decay time of  $\Delta\theta$ . Therefore, the ultrafast magnetization is related to the coherent charge motion, and its coherence time is consistent with the spectral bandwidths of SOC in-gap states ( $\sim 100$  meV). This oscillation survives even at 300 K, as shown by the blue circles in the inset of Fig. 3(e). This is consistent with the temperature-insensitive  $\Delta\theta$  up to 300 K (Supplemental Material 3 [21], Fig. S3)

Here, we theoretically study photo-induced dynamics of the spin and orbital degrees of freedom to analyze the mechanism for the photo-induced magnetization in  $\alpha$ -RuCl<sub>3</sub>. We consider a Hubbard model consisting of  $d_{yz}$ ,  $d_{xz}$ , and  $d_{xy}$  orbitals on each site of the honeycomb lattice [43–45], shown in Fig. 4(a) (Supplemental Material 10 [21]) [48,49]. Figure 4(b)



shows calculated linear optical conductivity ( $\sigma$ ) spectra for  $||a$  and  $||b$ . Below the Mott gap of  $\sim 1$  eV, some infrared peaks are found in the spectra. They are attributed to excitations from  $J_{\text{eff}} = \frac{3}{2}$  to  $\frac{1}{2}$  states [32–34] (Supplemental Material 10 [21]). Because of the finite-sized effect, the excitation spectra are quite discrete even above the Mott gap. The pseudospin dynamics are calculated based on numerical solutions to the time-dependent Schrödinger equation. Photo-excitation by a circularly polarized pulse is introduced through the Peierls phase (Supplemental Material 10 [21]) [48,49]. The magnetization  $M_{\text{ph}}$  [Fig. 4(c)] in the direction of  $\perp ab$  is given by  $M_{\text{ph}} = -2\mathbf{j}_{\perp}^{(1/2)}$ , where the pseudospin density  $\mathbf{j}^{(1/2)}$  is defined in Supplemental Material 10 [21]. The helicity-dependent  $M_{\text{ph}}$  grows during the excitation of 96 fs (=pulse width) with  $\hbar\omega = 0.3$  or 0.6 eV, showing that the magnetization arises within the pulse width (where the direction of  $M_{\text{ph}}$  is from the back to the front of Fig. 4(a) for  $\sigma^+$ ).

To interpret the photo-induced dynamics, we use a high-frequency expansion in the framework of quantum Floquet theory to evaluate an effective magnetic field. This effective

field emerges from the commutators among the kinetic operators on the three bonds (Supplemental Material 11 [21]) [50]. Thus, the charge hopping between different  $t_{2g}$  orbitals ( $d_{yz}-d_{xz}-d_{xy}$ ) [Fig. 4(a)] is essential to the photo-induced magnetization. The reduction of the ultrafast magnetization below  $T_N$  indicates that the interorbital charge motion is affected by pseudospin rotational symmetry breaking in the AFM phase. The coherent charge response in Fig. 3(e) shows a very important perspective for coherent control of the light-induced magnetization.

In summary, in this letter, we demonstrate the ultrafast magnetization in the multiorbital electron system  $\alpha$ - $\text{RuCl}_3$  by measuring the helicity-dependent polarization rotation. The light-induced magnetization is induced by the charge motion between different  $t_{2g}$  orbitals.

This letter was supported by JST, CREST (JPMJCR1901), Q-LEAP (JPMXS0118067426), and JSPS KAKENHI (20K03800, 18H01144, 20H05147, 22H00102, 20H01850, 19H05823, 19H05822, and 22H01175).

- 
- [1] H. Aoki, N. Tsuji, M. Eckstein, M. Kollar, T. Oka, and P. Werner, Nonequilibrium dynamical mean-field theory and its applications, *Rev. Mod. Phys.* **86**, 779 (2014).
- [2] C. Giannetti, M. Capone, D. Fausti, M. Fabrizio, F. Parmigiani, and D. Mihailovic, Ultrafast optical spectroscopy of strongly correlated materials and high-temperature superconductors: a non-equilibrium approach, *Adv. Phys.* **65**, 58 (2016).
- [3] D. N. Basov, R. D. Averitt, and D. Hsieh, Towards properties on demand in quantum materials, *Nat. Mater.* **16**, 1077 (2017).
- [4] T. F. Nova, A. Cartella, A. Cantaluppi, M. Först, D. Bossini, R. V. Mikhaylovskiy, A. V. Kimel, R. Merlin, and A. Cavalleri, An effective magnetic field from optically driven phonons, *Nat. Phys.* **13**, 132 (2017).
- [5] M. Cammarata, S. Zerdane, L. Balducci, G. Azzolina, S. Mazerat, C. Exertier, M. Trabuco, M. Levantino, R. Alonso-Mori, J. M. Glowia *et al.*, Charge transfer driven by ultrafast spin transition in a CoFe Prussian blue analogue, *Nat. Chem.* **13**, 10 (2021).
- [6] S. Koshihara, T. Ishikawa, Y. Okimoto, K. Onda, R. Fukaya, M. Hada, Y. Hayashi, S. Ishihara, and T. Luty, Challenges in developing a new class of photoinduced phase transition (PIPT): a step from classical to quantum PIPT, *Phys. Rep.* **942**, 1 (2022).
- [7] A. Kitaev, Anyons in an exactly solved model and beyond, *Ann. Phys.* **321**, 2 (2006).
- [8] G. Jackeli and G. Khaliullin, Mott Insulators in the Strong Spin-Orbit Coupling Limit: From Heisenberg to a Quantum Compass and Kitaev Models, *Phys. Rev. Lett.* **102**, 017205 (2009).
- [9] S. M. Winter, A. A. Tsirlin, M. Daghofer, J. van den Brink, Y. Singh, P. Gegenwart, and R. Valentí, Models and materials for generalized Kitaev magnetism, *J. Phys.: Condens. Matter* **29**, 493002 (2017).
- [10] H. Takagi, T. Takayama, G. Jackeli, G. Khaliullin, and S. E. Nagler, Concept and realization of Kitaev quantum spin liquid, *Nat. Rev. Phys.* **1**, 264 (2019).
- [11] A. Kirilyuk, A. V. Kimel, and T. Rasing, Ultrafast optical manipulation of magnetic order, *Rev. Mod. Phys.* **82**, 2731 (2010).
- [12] T. Kampfrath, K. Tanaka, and K. A. Nelson, Resonant and nonresonant control over matter and light by intense terahertz transients, *Nat. Photon.* **7**, 680 (2013).
- [13] P. Němec, M. Fiebig, T. Kampfrath, and A. V. Kimel, Antiferromagnetic opto-spintronics, *Nat. Phys.* **14**, 229 (2018).
- [14] T. Satoh, S.-J. Cho, R. Iida, T. Shimura, K. Kuroda, H. Ueda, Y. Ueda, B. A. Ivanov, F. Nori, and M. Fiebig, Spin Oscillation in Antiferromagnetic NiO Triggered by Circularly Polarized Light, *Phys. Rev. Lett.* **105**, 077402 (2010).
- [15] L. J. Sandilands, Y. Tian, K. W. Plumb, Y.-J. Kim, and K. S. Burch, Scattering Continuum and Possible Fractionalized Excitations in  $\alpha$ - $\text{RuCl}_3$ , *Phys. Rev. Lett.* **114**, 147201 (2015).
- [16] A. Banerjee, J. Yan, J. Knolle, C. A. Bridges, M. B. Stone, M. D. Lumsden, D. G. Mandrus, D. A. Tennant, R. Moessner, and S. E. Nagler, Neutron scattering in the proximate quantum spin liquid  $\alpha$ - $\text{RuCl}_3$ , *Science* **356**, 1055 (2017).
- [17] A. Little, L. Wu, P. Lampen-Kelley, A. Banerjee, S. Patankar, D. Rees, C. A. Bridges, J.-Q. Yan, D. Mandrus, S. E. Nagler *et al.*, Antiferromagnetic Resonance and Terahertz Continuum in  $\alpha$ - $\text{RuCl}_3$ , *Phys. Rev. Lett.* **119**, 227201 (2017).
- [18] J. Nasu, J. Knolle, D. L. Kovrizhin, Y. Motome, and R. Moessner, Fermionic response from fractionalization in an insulating two-dimensional magnet, *Nat. Phys.* **12**, 912 (2016).
- [19] Y. Kasahara, T. Ohnishi, Y. Mizukami, O. Tanaka, S. Ma, K. Sugii, N. Kurita, H. Tanaka, J. Nasu, Y. Motome *et al.*, Majorana quantization and half-integer thermal quantum hall effect in a Kitaev spin liquid, *Nature (London)* **559**, 227 (2018).
- [20] K. W. Plumb, J. P. Clancy, L. J. Sandilands, V. V. Shankar, Y. F. Hu, K. S. Burch, H.-Y. Kee, and Y.-J. Kim,  $\alpha$ - $\text{RuCl}_3$ : a spin-orbit assisted mott insulator on a honeycomb lattice, *Phys. Rev. B* **90**, 041112(R) (2014).
- [21] See Supplemental Material at <http://link.aps.org/supplemental/10.1103/PhysRevResearch.4.L032032> for (1) variation of  $T_N$  depending on crystalline polymorph, (2) dependence of  $\Delta\theta$  on ellipticity of pump pulse, (3) temperature dependence of  $\Delta\theta > 20$  K, (4) helicity-independent slow component of  $\Delta\theta$ ,

- (5)  $\Delta\theta$  measurement under excitation of 1.55 eV (across the Mott gap), (6) photocarrier generation induced by excitation below Mott gap, (7) calculated optical conductivity spectra for different values of SOI (synergy of onsite Coulomb interaction and SOI), (8) analysis of time evolutions of  $\Delta T/T$  and  $\Delta R/R$  by multi-exponential function, (9) ultrafast carrier dynamics captured by 6 fs pulse, (10) details of theoretical calculations: model and parameters, and (11) details of theoretical analysis: high-frequency expansion in Floquet theory.
- [22] J. A. Sears, M. Songvilay, K. W. Plumb, J. P. Clancy, Y. Qiu, Y. Zhao, D. Parshall, and Y.-J. Kim, Magnetic order in  $\alpha$ -RuCl<sub>3</sub>: a honeycomb-lattice quantum magnet with strong spin-orbit coupling, *Phys. Rev. B* **91**, 144420 (2015).
- [23] Y. Kubota, H. Tanaka, T. Ono, Y. Narumi, and K. Kindo, Successive magnetic phase transitions in  $\alpha$ -RuCl<sub>3</sub>: XY-like frustrated magnet on the honeycomb lattice, *Phys. Rev. B* **91**, 094422 (2015).
- [24] R. D. Johnson, S. C. Williams, A. A. Haghighirad, J. Singleton, V. Zapf, P. Manuel, I. I. Mazin, Y. Li, H. O. Jeschke, R. Valentí *et al.*, Monoclinic crystal structure of  $\alpha$ -RuCl<sub>3</sub> and the zigzag antiferromagnetic ground state, *Phys. Rev. B* **92**, 235119 (2015).
- [25] H. B. Cao, A. Banerjee, J.-Q. Yan, C. A. Bridges, M. D. Lumsden, D. G. Mandrus, D. A. Tennant, B. C. Chakoumakos, and S. E. Nagler, Low-temperature crystal and magnetic structure of  $\alpha$ -RuCl<sub>3</sub>, *Phys. Rev. B* **93**, 134423 (2016).
- [26] S.-Y. Park, S.-H. Do, K.-Y. Choi, D. Jang, T.-H. Jang, J. Schefer, C.-M. Wu, J. S. Gardner, J. M. S. Park, J.-H. Park *et al.*, Emergence of the isotropic Kitaev honeycomb lattice with two-dimensional Ising universality in  $\alpha$ -RuCl<sub>3</sub>, [arXiv:1609.05690v1](https://arxiv.org/abs/1609.05690v1).
- [27] A. Glamazada, P. Lemmens, S.-H. Do, Y. S. Kwon, and K.-Y. Choi, Relation between Kitaev magnetism and structure in  $\alpha$ -RuCl<sub>3</sub>, *Phys. Rev. B* **95**, 174429 (2017).
- [28] Y. Nagai, T. Jinno, J. Yoshitake, J. Nasu, Y. Motome, M. Itoh, and Y. Shimizu, Two-step gap opening across the quantum critical point in the Kitaev honeycomb magnet  $\alpha$ -RuCl<sub>3</sub>, *Phys. Rev. B* **101**, 020414(R) (2020).
- [29] J. A. Sears, Y. Zhao, Z. Xu, J. W. Lynn, and Y.-J. Kim, Phase diagram of  $\alpha$ -RuCl<sub>3</sub> in an in-plane magnetic field, *Phys. Rev. B* **95**, 180411(R) (2017).
- [30] L. Wu, A. Little, E. E. Aldape, D. Rees, E. Thewalt, P. Lampen-Kelley, A. Banerjee, C. A. Bridges, J.-Q. Yan, D. Boone *et al.*, Field evolution of magnons in  $\alpha$ -RuCl<sub>3</sub> by high-resolution polarized terahertz spectroscopy, *Phys. Rev. B* **98**, 094425 (2018).
- [31] L. J. Sandilands, Y. Tian, A. A. Reijnders, H.-S. Kim, K. W. Plumb, Y.-J. Kim, H.-Y. Kee, and K. S. Burch, Spin-orbit excitations and electronic structure of the putative Kitaev magnet  $\alpha$ -RuCl<sub>3</sub>, *Phys. Rev. B* **93**, 075144 (2016).
- [32] P. Warzanowski, N. Borgwardt, K. Hopfer, J. Attig, T. C. Koethe, P. Becker, V. Tsurkan, A. Loidl, M. Hermanns, P. H. M. van Loosdrecht *et al.*, Multiple spin-orbit excitons and the electronic structure of  $\alpha$ -RuCl<sub>3</sub>, *Phys. Rev. Research* **2**, 042007(R) (2020).
- [33] J.-H. Lee, Y. Choi, S.-H. Do, B. H. Kim, M.-J. Seong, and K.-Y. Choi, Multiple spin-orbit excitons in  $\alpha$ -RuCl<sub>3</sub> from bulk to atomically thin layers, *npj Quantum Mater.* **6**, 43 (2021).
- [34] A. Loidl, P. Lunkenhaimer, and V. Tsurkan, On the proximate Kitaev quantum-spin liquid  $\alpha$ -RuCl<sub>3</sub>: thermodynamics, excitations and continua, *J. Phys.: Condens. Matter* **33**, 443004 (2021).
- [35] Y. Hasegawa, T. Aoyama, K. Sasaki, Y. Ikemoto, T. Moriwaki, T. Shirakura, R. Saito, Y. Imai, and K. Ohgushi, Two-phonon absorption spectra in the layered honeycomb compound  $\alpha$ -RuCl<sub>3</sub>, *J. Phys. Soc. Jpn.* **86**, 123709 (2017).
- [36] Y. Kawakami, T. Amano, Y. Yoneyama, Y. Akamine, H. Itoh, G. Kawaguchi, H. M. Yamamoto, H. Kishida, K. Itoh, T. Sasaki *et al.*, Nonlinear charge oscillation driven by a single-cycle light field in an organic superconductor, *Nat. Photon.* **12**, 474 (2018).
- [37] Y. Kawakami, T. Amano, H. Ohashi, H. Itoh, Y. Nakamura, H. Kishida, T. Sasaki, G. Kawaguchi, H. M. Yamamoto, K. Yamamoto *et al.*, Petahertz non-linear current in a centrosymmetric organic superconductor, *Nat. Commun.* **11**, 4138 (2020).
- [38] Yu. P. Svirko and N. I. Zheludev, *Polarization of Light in Nonlinear Optics* (Wiley-VCH, 1998).
- [39] R. V. Mikhaylovskiy, E. Hendry, and V. V. Kruglyak, Ultrafast inverse faraday effect in a paramagnetic terbium gallium garnet crystal, *Phys. Rev. B* **86**, 100405(R) (2012).
- [40] R. B. Versteeg, A. Chiochetta, F. Sekiguchi, A. Sahasrabudhe, J. Wagner, A. I. R. Aldea, K. Budzinauskas, Z. Wang, V. Tsurkan, A. Loidl *et al.*, Nonequilibrium quasistationary spin disordered state in  $\alpha$ -RuCl<sub>3</sub>, *Phys. Rev. B* **105**, 224428 (2022).
- [41] C. S. Wang and J. Callaway, Band structure of nickel: spin-orbit coupling, the fermi surface, and the optical conductivity, *Phys. Rev. B* **9**, 4897 (1974).
- [42] D. Nevola, A. Bataller, A. Kumar, S. Sridhar, J. Frick, S. O'Donnell, H. Ade, P. A. Maggard, A. F. Kemper, K. Gundogdu *et al.*, Timescales of excited state relaxation in  $\alpha$ -RuCl<sub>3</sub>, observed by time-resolved two-photon spectroscopy, *Phys. Rev. B* **103**, 245105 (2021).
- [43] J. G. Rau, E. K. -H. Lee, and H.-Y. Kee, Generic Spin Model for the Honeycomb Iridates Beyond the Kitaev Limit, *Phys. Rev. Lett.* **112**, 077204 (2014).
- [44] H.-S. Kim and H.-Y. Kee, Crystal structure and magnetism in  $\alpha$ -RuCl<sub>3</sub>: An *ab initio* study, *Phys. Rev. B* **93**, 155143 (2016).
- [45] S. M. Winter, Y. Li, H. O. Jeschke, and R. Valentí, Challenges in design of Kitaev materials. Magnetic interactions from competing energy scales, *Phys. Rev. B* **93**, 214431 (2016).
- [46] Y. Kawakami, T. Fukatsu, Y. Sakurai, H. Unno, H. Itoh, S. Iwai, T. Sasaki, K. Yamamoto, K. Yakushi, and K. Yonemitsu, Early-Stage Dynamics of Light-Matter Interaction Leading to the Insulator-to-Metal Transition in a Charge Ordered Organic Crystal, *Phys. Rev. Lett.* **105**, 246402 (2010).
- [47] T. Ishikawa, Y. Sagae, Y. Naitoh, Y. Kawakami, H. Itoh, K. Yamamoto, K. Yakushi, H. Kishida, T. Sasaki, S. Ishihara *et al.*, Optical freezing of charge motion in an organic conductor, *Nat. Commun.* **5**, 5528 (2014).
- [48] K. Yonemitsu, S. Miyashita, and N. Maeshima, Photoexcitation-energy-dependent transition pathways from a dimer mott insulator to a metal, *J. Phys. Soc. Jpn.* **80**, 084710 (2011).
- [49] K. Yonemitsu and N. Maeshima, Coupling-dependent rate of energy transfer from photoexcited Mott insulators to lattice vibrations, *Phys. Rev. B* **79**, 125118 (2009).
- [50] A. Eckardt and E. Anisimovas, High-frequency approximation for periodically driven quantum systems from a Floquet-space perspective, *N. J. Phys.* **17**, 093039 (2015).